J Mar Sci Technol (2014) 19:338–350
DOI 10.1007/s00773-013-0252-z

ORIGINAL ARTICLE

An experimental study on water entry of horizontal cylinders

Zhaoyu Wei · Changhong Hu

Received: 26 July 2013 / Accepted: 28 December 2013 / Published online: 24 January 2014

Abstract Complex hydrodynamics of a circular cylinder entering into water horizontally for low Froude numbers is experimentally studied. A high-speed digital video camera system is used to record the water entry process. The emphasis of this study is to investigate the three-dimensional effect on the water entry of the horizontal cylinders. A new experimental setup is built for this purpose and great effort is put on taking high quality pictures of the free surfaces. In the experiment four length to diameter ratios, two cylinder-water density ratios, and two release heights are investigated. For comparison, experiment with a sphere is also carried out. Quantitative analysis is performed based on the digital video images and the results are presented. The results obtained from this study can be used not only for understanding the physics but also for the purpose of validation of numerical models.

Keywords Water entry · Horizontal cylinder · Three-dimensional effect · Cavity dynamics

Z. Wei
Interdisciplinary Graduate School of Engineering Sciences, Kyushu University, Kasuga, Fukuoka 816-8580, Japan

Present Address:
Z. Wei
School of Mechanical and Aerospace Engineering, Nanyang Technological University, Singapore, Singapore

C. Hu (✉)
Research Institute for Applied Mechanics, Kyushu University, Kasuga, Fukuoka 816-8580, Japan
e-mail: hu@riam.kyushu-u.ac.jp

1 Introduction

The water entry events have been of interest for the scientists for over 100 years. Worthington and Cole [1] used single-spark photography and presented an initial image of water impact cavity and splash. Quantitative experimental work on measuring the impact force as object entering water started from Watanabe [2]. After that, the water entry investigation was mainly performed for design of military projectiles at high speed [3–8] and the Dam Busters [9]. Subsequent research on these kinds of impacts arises in much wider interests and applications, for example, in the crater mechanics [10, 11], locomotion of basilisk lizards [12], granular impacts [13–15] and skipping stones [16]. Recently, most of the investigations aim to reveal the physics of impact cavities [17–20].

When a sphere impacts the water surface with sufficiently high velocity, a small horizontal jetting is ejected from the impact point at the initial stage. Thoroddsen et al. [21] found that this initial axisymmetric jetting can emanates radially outwards at a speed up to 30 times of sphere's velocity. He also found the initial jetting forms within 1 ms from the first contact and mostly within the first 100 μs.

As regard to the cavity dynamics, there are a few key mechanisms driving surface closure. Gilbarg and Anderson [22] considered that the atmosphere pressure is an important factor, and they concluded that the time to surface closure is inversely proportional to the atmosphere pressure. Other key mechanisms are addressed by Lee et al. [23] as Bernoulli pressure and surface tension. As the cavity grows, air flow in through the splash curtain, then the splash curtain domes over and closes. For water entry with low Froude numbers, both the inertia and gravity effects are relevant to the deep closure, which eventually

occurs when cavity expanding radially is retarded by the hydrostatic pressure of the surrounding fluid.

Typical images for the free surface deformation by the water entry of two-dimensional cylinders were firstly presented by Greenhow and Lin [24]. In their work, the length of the cylinders is almost the same with that of the tank. As the cylinder impacts on the water surface, a clear two-dimensional cavity is created. In Greenhow and Lin' experimental, the water depth is shallow, which could not present us a whole cavity revolution for the horizontal cylinders.

In this research, we design a new experimental setup to investigate the water entry phenomena with a horizontal circular cylinder. The three-dimensional effect on the free surface impact and cavity dynamics, which has not well studied so far, is our research interest. Length to diameter ratio, cylinder-water density ratio, and impact velocity are chosen as the experimental parameters. Experiment on a sphere is also performed for comparison. One objective of this research is to obtain clear pictures in the experiment for investigation of three-dimensional cavity dynamics. The organization of this paper is as follows. In Sect. 2 the experimental setup is described in details. A lot of effort has been addressed for the experimental methods and system. In Sect. 3, the results obtained from the experiment are presented and discussed. The effect of two parameters on the water entry, the geometry ratio of cylinder length to diameter and the density ratio of cylinder to water, is discussed quantitatively. In the last section, conclusions obtained through this study are provided.

2 Experimental setup

The experiment was conducted in Research Institute for Applied Mechanics (RIAM), Kyushu University, Japan. During the experiment, the room temperature varied between 21 and 26 °C. Details on the experiment are described in this section.

2.1 The water tank and release mechanism

A schematic illustration of our experimental apparatus is shown in Fig. 1a. The cylinders (diameter $d = 50$ mm) are released horizontally into a tank with quiescent water. The tank is of cubic shape with length of 1.35 m for each side. The water depth is 1.0 m. The tank is made by acrylic plates with the thickness of 2.0 cm, which is reinforced by using acrylic bars at the four vertical corners and steel bars at the bottom. When the tank is filled with water, the

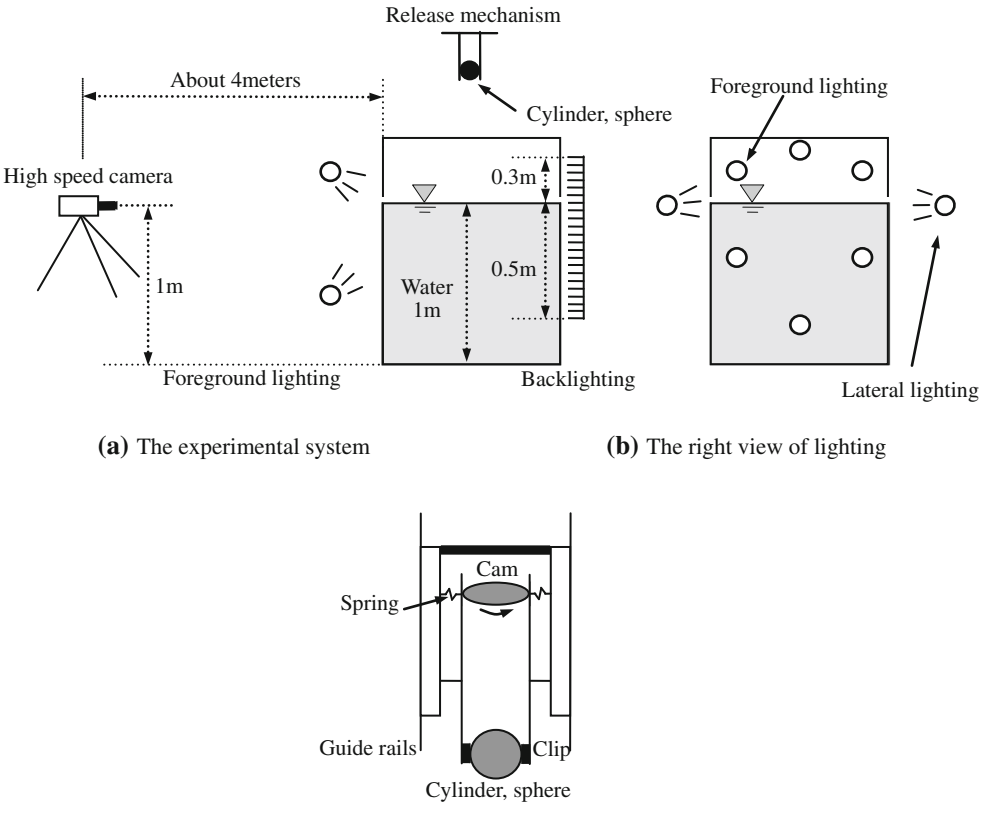

(a) The experimental system

(b) The right view of lighting

(c) The release mechanism

Fig. 1 Schematic illustration of the experimental apparatus

deformation of the wall is small enough so that the light refraction error caused by the tank deformation can be neglected.

During the experiment, it is difficult to let the cylinder impact water surface totally horizontally. A very small inclined angle or rotation will make it difficult to observe the initial impact behaviors, as well as evaluating the speed of initial jetting. Thus repeatable impact conditions are very important. For this purpose, a new release mechanism is designed, as shown in Fig. 1c, which is like a clamp. The release mechanism is installed along a pair of glide rails above the tank so that the height of the cylinders can be adjusted. As the cam is rotated by a switch, two strong springs will push the upper ends of two clamp beams quickly inside, and then the cylinders will be released into the tank freely. The contact points of the cam with clamp beams are lubricated to keep the contact points smooth, so that no vibration and rotation is caused when releasing the cylinders. No matter how we improve the release mechanism as well as possible, it is still very difficult to keep a right horizontal pose for each time. So each impact case is repeated for many times, and then the best one is chosen to analyze the cavity formation and several better cases are chosen to calculate the speed of initial jetting. The jetting speed value for each case is calculated with an average scale to suppress the error.

2.2 The cylinders

Solid circular cylinders of two materials, Polyvinyl chloride and Polypropylene, are used. Two release height of $H_0 = 1.0$ and 2.0 m with the center of the cylinders above water are considered. The water entry with a cylinder can be characterized by four non-dimensional parameters: Reynolds number $Re = U_0 d/\nu$, Weber number $W = \rho U_0^2 R_0/\sigma$, Bond number $B = \rho g R_0^2/\sigma$, and Froude number $Fr = U_0/\sqrt{gd}$. Here, U_0 is the initial impact velocity; R_0 is the radius of the cylinder. The properties of the water are density $\rho \approx 1000$ kg/m^3, surface tension $\sigma \approx 0.07$ kg/s^2, and kinematic viscosity $\nu \approx 10^{-6}$m^2/s. The parameters used in the experiment are shown in Table 1. In addition, the ratio of the cylinder's length to its diameter is defined as L/d, and the density ratio of the solid to water is defined as $D = \rho_{\text{solid}}/\rho_{\text{water}}$, where ρ_{solid} is the density of the cylinder with even density distribution. The diameter of all cylinders is $d = 50$ mm, and the lengths of the cylinders are chosen as $L = 25$, 50, 100 and 200 mm to have the ratios L/d of 0.5, 1, 2 and 4, respectively. The density ratios are $D = 1.37$ and 0.90 for cylinders with two different materials. For the purpose of comparison, experiment on two spheres with diameter of $d = 50$ mm and the density ratio of $D = 1.37$ and 0.90 is also carried out.

Table 1 Parameters for water entry experiment

H_0 (m)	$W = \rho U_0^2 R_0/\sigma$	$B = \rho g R_0^2/\sigma$	$Re = U_0 d/\nu$	$Fr = U_0/\sqrt{gd}$
1.0	6.65×10^3	87.5	2.16×10^5	6.25
2.0	1.37×10^4	87.5	3.09×10^5	8.89

As shown in Table 1, the present experiment is conducted in the region of high Reynolds and Weber numbers, moderate Bond number and low Froude numbers. Further, the viscosity and surface tension play a marginal role in the formation of cavities.

The cylinders and spheres have the same surface roughness, which is determined by machining process. During the experiment, the surface of the cylinders and spheres is only cleaned using the ethanol, no special treatment has been done. The surface roughness will affect the surface contact angle, and thus affect the cavity formation [27]. The sessile water drop method is used to test the static contact angle of the cylinders and spheres' surface. Several water drops are dropped on different places on the cylinder and sphere's surface, it provides us with an average value of $\theta_c = 98^\circ \pm 10^\circ$.

2.3 Lighting and photographing

The essential factor that influences the quality of experiment is the lighting. In the experiment, backlighting, foreground lighting and lateral lighting are used (Fig. 1a, b). We use the standard RIFA-F 80 cm × 80 cm photography fluorescent light as the background lighting, which is positioned directly behind the impact zone outside of the tank, and projects light directly towards the camera. The backlighting can create a uniform and white backdrop, which particularly helps highlight the splash and cavity formation. When strong backlighting is applied, the cavity and splash will be obviously outlined as dark shadows for the varying index of refraction of the water disturbed by cavities. Then, we use six 500 W PRF flood bulbs as the foreground lighting to illuminate the dark shadows from the front. The foreground lighting is shown in Fig. 1b, which form an approximate hexagon circle around the center of impact region, three below the water surface and three above water surface. For the long cylinders, we need more information about the cavity flows. Thus two 500 W PRF flood lights are used as the lateral lighting to illuminate the cavity and splash from the two sides. The lighting system is adjusted to its best condition for each test.

A high-speed digital video camera (Photron FASTCAM-APX RS) with a 105 mm, *f*/2.8 Micro Nikon lens is used in the experiment. The height of the length is set the same with the water surface. The lens opening is set to its maximum. The frame rate is set to 1000 fps for color images with the full resolution of 1024(H) × 1024(V) pixels. When very strong

lighting is applied, we can decrease the exposure time as low as possible to get clear images. In the experiment, the shutter speed is set as 1/3000 s and a fixed field of view (FOV) is used for all cases.

When taking the images of jetting, the lens is set slightly higher than the still water surface and as close as to the tank. Only the very strong backlighting is used while all the foreground lightings and lateral lightings are turned off. The frame rate of the camera is set to 20000 fps, corresponding to the resolution of 256(H) × 512(V) pixels. Each experimental case is repeated for several times.

2.4 Position extraction and jetting speed calculation

The position of the cylinders is extracted from each frame of the image sequence using the method of Digital Image Correlation (DIC) in which the Gaussian Distribution Fitting is applied to get the sub pixel positions. Then the raw data are smoothed using a quintic spline smoothing scheme. The method in the present work is similar with that used by Truscott [25]. In the DIC procedure, at first the image with the object above the water surface is used to form a template. The cylinder in the water shows about four pixels larger than that in the air due to lighting refraction. To extract the positions as accurately as possible, the template is modified so that the size of the circular shape is the same as seen in the water. Then the template is cross correlated to the images in the sequence to get the pixel position of the object. Due to the error caused by lighting refraction, the ± 0.5 pixels, which yields an uncertainty of $\pm 3.52 \times 10^{-4}$ m in vertical position.

The speed of the initial jetting is directly evaluated through the pixel displacement of the jetting between two continuous images in a sequence. In each frame of a image sequence, the pixel position of the jetting tip at the two sides are known, the pixel difference of the jetting tips between two continuous images is the pixel displacement between the two frames. When considered the real time interval and the amplified coefficient, the jetting speed could be estimated. We first average the jetting speed over several frames to get the jetting speed in this image sequence, and then average the jetting speed over several sequences to get the final jetting speed, aiming to suppress the error. The error for the initial jetting's speed is estimated to be within 10 %.

3 Experiment results and discussion

3.1 Water entry with long horizontal cylinder

Figures 2 and 3 show the time series of photography for the case of $D = 1.37$ and $L/d = 4$ from the right view and the side view, respectively. The two sets of figure are synchronized in time. At the time of $t_0 = 0$ s, the object touches the water surface. The initial impact velocity of the cylinder is $U_0 = 6.22$ m/s ($Fr = 8.89$). The formation and closure of the cavities are mainly dominated by the inertial effect and hydrostatic pressure. Several new phenomena can be addressed.

3.1.1 The initial high-speed jetting

In the initial stage of impact, when the cylinder touches the water surface, the part of water occupied by the cylinder is ejected at the point of contact. A high-speed horizontal jetting at the two sides can be clearly seen in Fig. 2a, which is more evident than that of a sphere as described by Truscott and Techet [25]. The jetting extends almost horizontally outwards as the cylinder descends into water. For the long cylinder, the initial wing-shaped jetting is emitted approximately two-dimensionally. As observed in Fig. 3a, the spray jetting formed at the two ends is too weak to be observed, compared to these at the two sides.

3.1.2 The open cavity

In Fig. 2c, an open air cavity is formed behind the cylinder. The thin water layer and the cavity lip grow in size. The tails of the thin water layer, as mentioned above as the initial jetting move with very high speed and finally break up from the thin water layer into small drops of spray, which fly outside the camera's field of view (Fig. 2c). The reduced air pressure in the cavity draws the splash moving inwards [23]. At the same time, the splash grows upward forming an approximately vertical curtain, also known as the splash crown in Figs. 2d and 3d. All over the frames, the splash curtain cannot dome over as that of a vertical sphere [25].

3.1.3 The cavity shape inversion behavior

In Fig. 2d, as the entire cylinder passes below the ambient free surface, the flows separated from the cylinder surface in the side direction and right direction form four obvious cross lines. The two pairs of cross lines at each end of the cylinder move faster than other parts of the cavity and begin approaching to each other (Fig. 2c–e), and finally intersect at the time of t_{cp} (Fig. 2f). After the two pairs of cross lines close, two new cross lines are formed (Fig. 2f). They still move along the axis directions to each other faster than other parts of the cavity (Figs. 2f–h, 3f–h). This phenomenon is named as cavity shape inversion [26] and is more obvious in the cavity pinch-off cross section.

The schematic illustration for the cavity phase inversion behavior is shown in Fig. 4. A horizontal cross-section for the cavity when it is just formed is shown in Fig. 4a. Since the curvature is higher at the two ends of the cross-section,

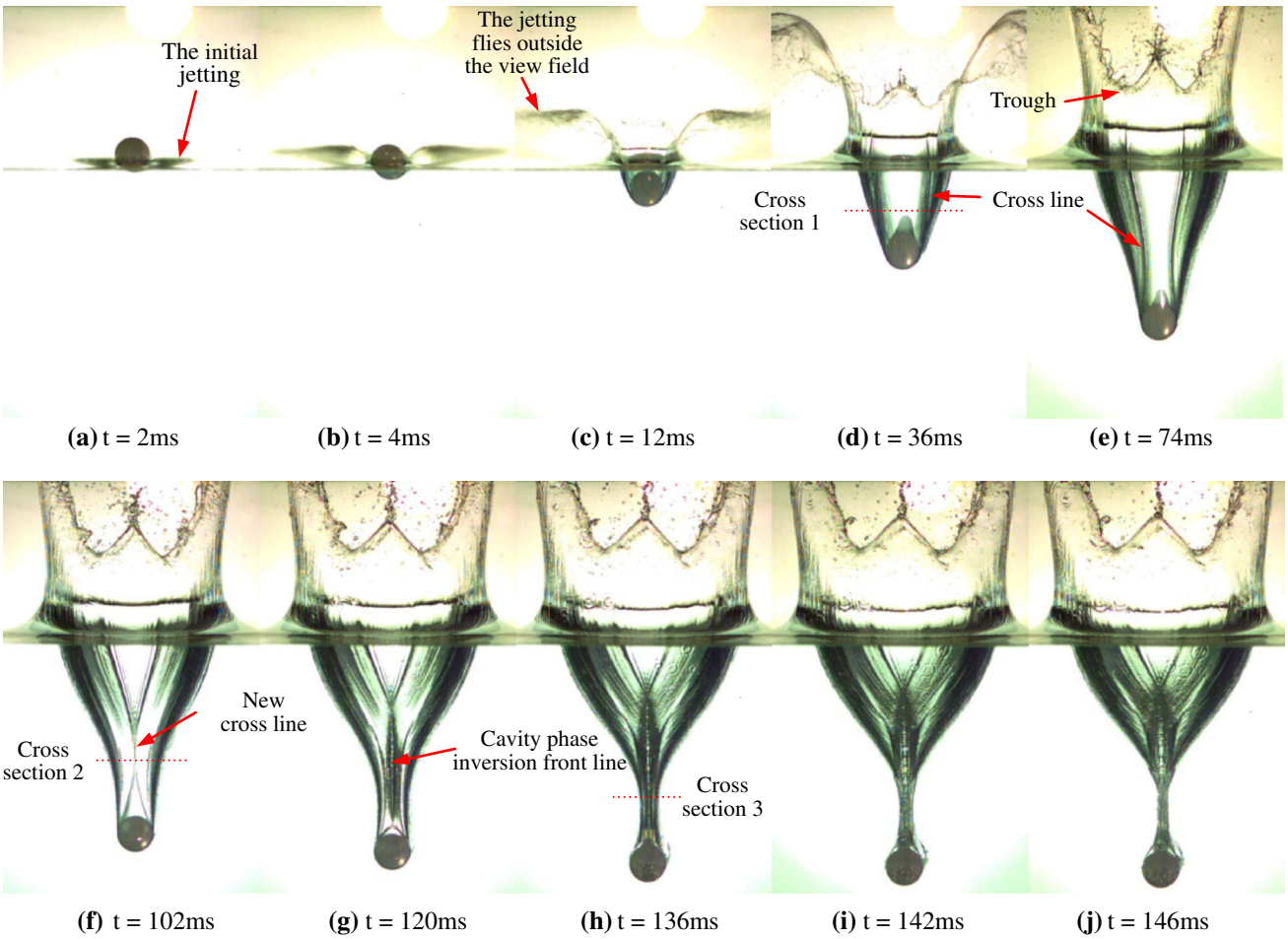

Fig. 2 A sequence of images describing the evolution of cavity and splash for the cylinder with $L/d = 4$, $D = 1.37$, entering water horizontally. It is taken from the front view along the axis. As released from a height of 2.0 m, the initial impact velocity is $U_0 = 6.22$ m/s ($Fr = 8.89$)

especially at the four cross lines, thus the acceleration along the cylinder's axis is larger in these parts. As the four cross lines intersect with each other, two new cross lines are formed Fig. 4b. Finally, the two new cross lines begin to move to each other with higher acceleration than other parts Fig. 4c and the cavity enters the inertial collapse regime.

3.1.4 The collapsing of the cavity

As shown in Figs. 2 and 3, for the long cylinder, two-dimensional flow occurs near the center of the cylinder with three-dimensional effects being important near the region of two ends. The three-dimensional region extends at a certain speed towards the central part. Towards the cavity pinch-off, the air is pushed out of the shrinking cavity at very high speed. Before the two front lines of cavity shape inversion meet each other, the cavity has already collapsed along the diameter directions. It finally breaks up into three parts (Fig. 3i).

3.2 The speeds of the initial horizontal jetting

It can be obviously observed in Fig. 2a that the initial horizontal jetting for a cylinder is much stronger than that formed by a sphere [25]. Using frame rate about 20 kfps, we can get an approximate evaluation for the speed of this jetting and its evolution. The selected image sequences of the jetting formed by a light cylinder ($L/d = 1$, $D = 0.90$), as well as a light sphere ($D = 0.90$) are shown in Fig. 5. As the camera is slightly higher than the still water surface, the reflected images of the jetting and the solid could be seen clearly in Fig. 5. The impact velocities for both the cylinder and the sphere are $U_0 = 6.22$ m/s. After about 200 μs, the initial impact stage finished, and the cylinder moves into the second stage [8]. A very thin water film is formed and then departs from the cylinder's surface. The wing-shaped sprays could be observed (Fig. 5a). Obviously, the initial jetting formed by the cylinder moves faster than that by the sphere.

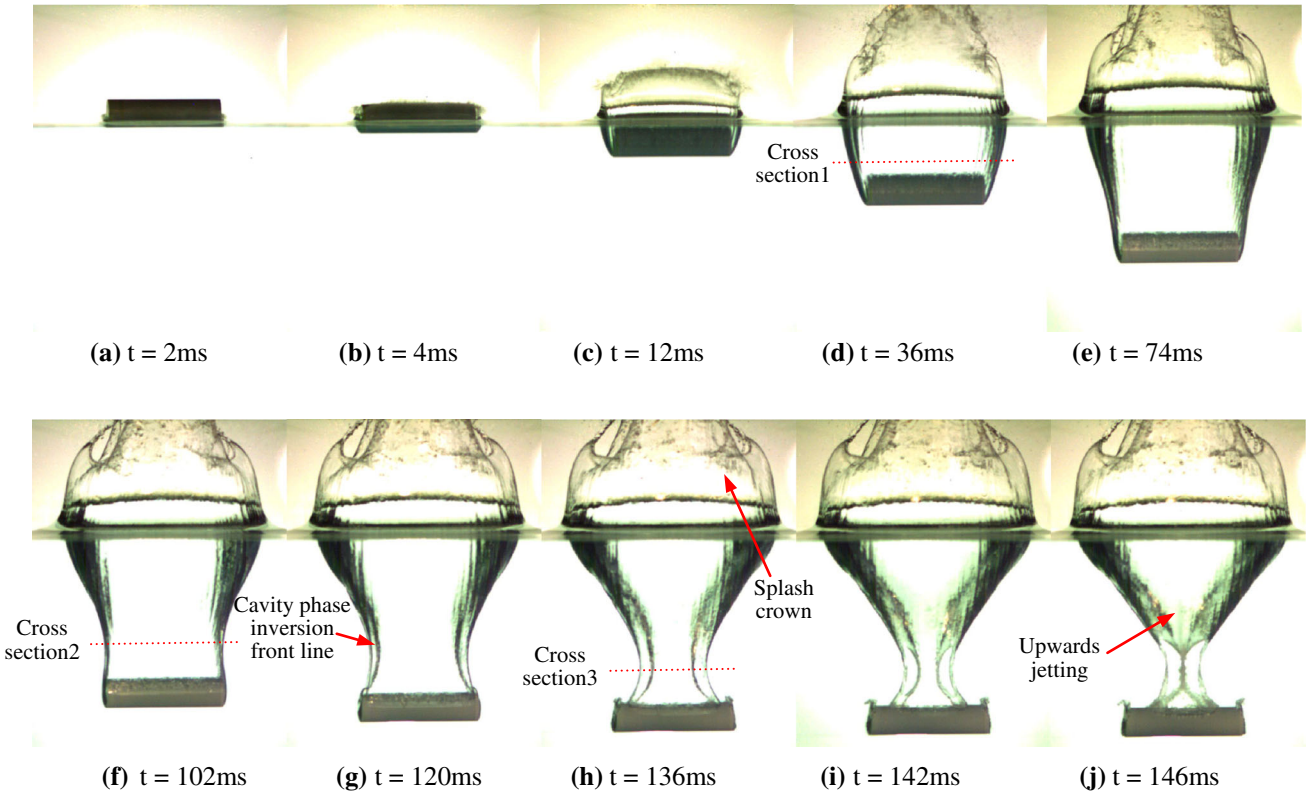

Fig. 3 A sequence of images describe the same case as that in Fig. 3 from the side view, which is synchronized with Fig. 3 in time

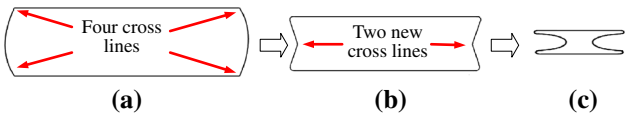

Fig. 4 Schematic illustration of the cavity shape inversion behaviors as the cavity collapses. **a** is the schematic horizontal cross section for the cavity shown in Figs. 2d and 3d; **b** is the cross section in Figs. 2f and 3f; **c** is for the cross section in Figs. 2h and 3h

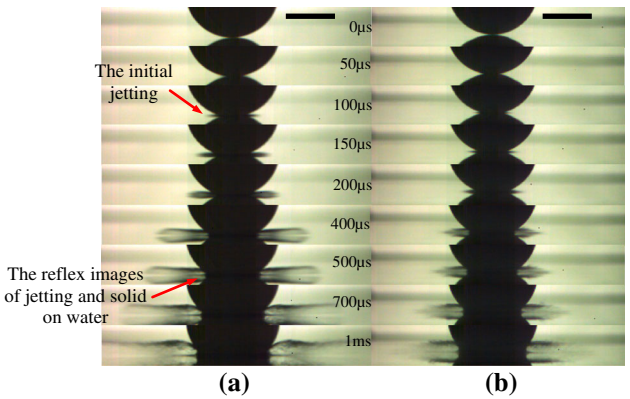

Fig. 5 Impact jetting and spray formed by the cylinder ($L/d = 1$, $D = 0.90$) (**a**) and sphere ($D = 0.90$) (**b**) with initial velocity of $U_0 = 6.22$ m/s. The two images sequences are synchronized in time. The *scale bars* are 25 mm long

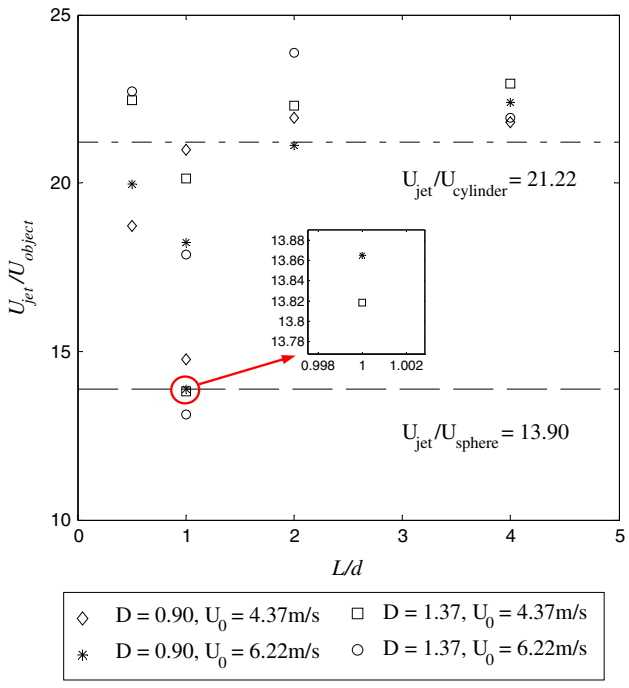

Fig. 6 The initial jetting speed normalized by impact velocity of cylinders and spheres, $U_{jetting}/U_{cylinder}$ versus the L/d

To further evaluating the speed of the jetting, both groups of cylinders, as well as spheres and two released heights (1.0 m, 2.0 m) are considered. The ratios of the jetting' speed to the speed of bodies, $U_{\text{jetting}}/U_{\text{cylinder}}$ versus the L/d, are calculated and shown in Fig. 6. It can be found that for all the cylinders this ratio is larger than these of spheres. The $U_{\text{jetting}}/U_{\text{cylinder}}$ for the cylinders has an average value of about 21.22, which is a reasonable value as mentioned by Thoroddsen et al. [21]. While this value for the sphere is just about 13.90. The speed of the jetting formed by a horizontal cylinder is about 1.5 times of that by a sphere, which is a reasonable number by consideration of two-dimensional jetting and three-dimensional jetting. The L/d and the density ratios considered here has little influence on the jetting speed.

3.3 The critical velocity for air entrainment

Similar to spheres [27], two-dimensional cylinders also need enough energy to form cavities. In Fig. 7, water entry of the horizontal cylinder with $L/d = 4$, $D = 1.37$ at impact velocity of $U_0 = 1.21$ m/s is shown. In this case the impact velocity is below the critical velocity to form a cavity. When the cylinder impacts the quiescent water surface, a thin liquid film develops (Fig. 7b). It does not separate from the cylinder's surface (Fig. 7c). After the entire cylinder passes the ambient free surface, there is no cavity found (Fig. 7d).

The right view of the case in Fig. 7 is shown in Fig. 8a1–a5. When the cylinder touches the water surface, an initial strong jetting can be seen at the two sides; and a thin water film is formed (Fig. 8a1). The jetting moves with very high speed and breaks up (Fig. 8a2). The water climbs up on the cylinder surface (Fig. 8a4), finally close up at the apex (Fig. 8a5). No cavity is formed.

In a contrary, the initial jetting formed by the sphere is weak, comparing to the cylinder with the same density ratio and impact velocity (Fig. 8b1–b5). As shown in Fig. 8, for the cylinder at 12 ms (Fig. 8a4) after impacting, the thin water film has already reached about 3/4 of its diameter, while for the sphere it is just a half way traveling (Fig. 8b3). At 22 ms after impacting (Fig. 8a5), the thin water films has already closed up at the apex for the cylinder, while for the sphere it has reached only about 3/4 of diameter (Fig. 8b4). The ratio of the speed of the thin water films by the cylinder to that by a sphere can be roughly evaluated as 1.5, which coincides with the results shown in Fig. 6.

Based on the above analysis, it could be noted here that the critical velocity for a cylinder is lower than that for a sphere. Figure 9 provides a comparison between a long cylinder ($L/d = 4$) and a sphere, with the density ratio of $D = 1.37$ and the impact velocity of $U_0 = 3.05$ m/s. The cylinder and the sphere have the same surface roughness, as well as the contact angle. It is found that the cavity only exists in the case of the cylinder.

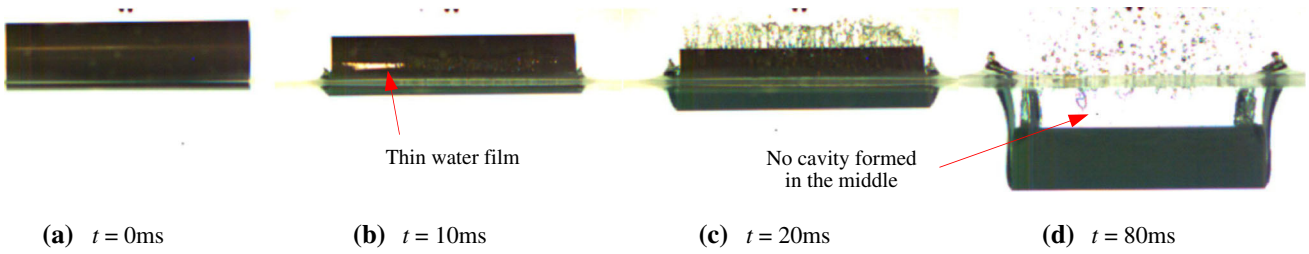

Fig. 7 A sequence of images as the cylinder with $L/d = 4$, $D = 1.37$, enters water horizontally with a low initial speed of $U_0 = 1.21$ m/s

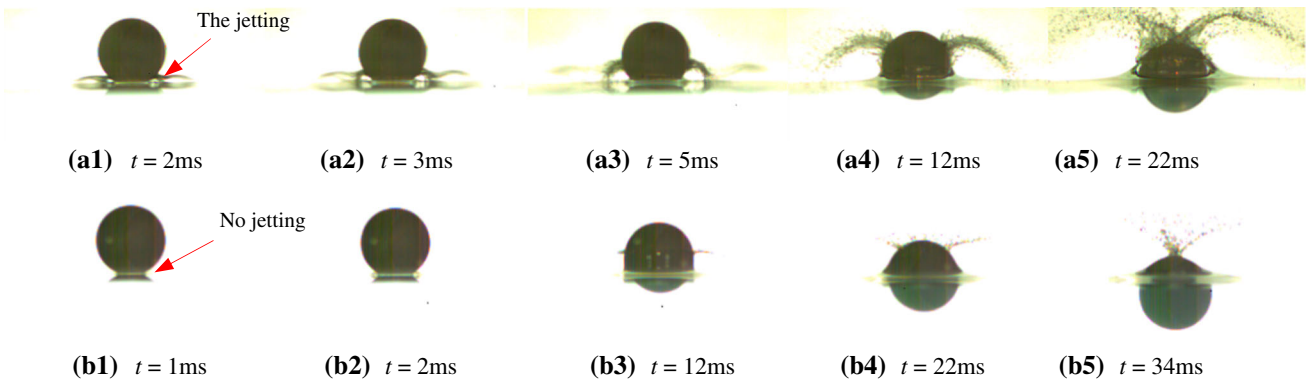

Fig. 8 Selected image sequences for the impact of a horizontal cylinder ($L/d = 4$, $D = 1.37$) (**a**) and a sphere ($D = 1.37$) (**b**) with a very low speed of $U_0 = 1.21$ m/s

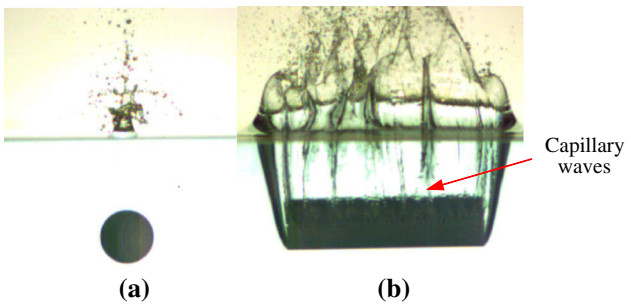

Fig. 9 The snapshots for the entry of a sphere ($D = 1.37$) (**a**) and a horizontal cylinder ($L/d = 4$, $D = 1.37$) (**b**) into water with $U_0 = 3.05$ m/s

3.4 Effect of length on the cavity and splash

For a horizontal cylinder entering into water, the ratio of the cylinder's length to its diameter (L/d) greatly affects the formation and evolution of the cavity and splash. The results for $L/d = 2$ and 1 are shown in this section for discussion of this aspect.

The initial spray jetting formed by the cylinders with $D = 1.37$ for $L/d = 2$ and 1, are shown in Fig. 10a, b, respectively. The initial impact velocity is 6.22 m/s. We could not observe obvious difference between the two groups of figures. Similar to the cylinder with $L/d = 4$ (Figs. 2a, 3a), very strong sprays can be observed at the two sides, and just weak sprays are formed at the two ends. The strength of the spray is increased with L/d.

For the long cylinder ($L/d = 4$), at 102 ms after impact, the cavity shape inversion behavior could be obviously observed in Fig. 3g–h. As the two cross lines of cavity shape inversion approach each other, the cavity shrinks along both the axis and diameter directions. Eventually before they meet each other, the cavity pinches off along the diameter direction and breaks up into three parts. As observed in Fig. 11a, for the cylinder with $L/d = 2$, the two cross lines meet each other before the cavity pinches off along the diameter direction, thus the cavity is cut into two parts along the axis direction, until then the two-dimensional flows in the center of the cylinder disappears at the time of 124 ms. From a side view, 2 ms later the cavity is still split into three parts and then all the three cavities pinch-off into bubbles line (not shown).

For the cylinder with $L/d = 1$, the cavity is also cut into two parts along the axis direction by the cross lines of cavity shape inversion, and the two parts of cavities both shrink into a point (Fig. 11b). The two-dimensional flows disappears at time of 106 ms. Another phenomenon could be noticed is that the ripples as the cavity collapses for the small cylinder ($L/d = 1$) (Fig. 12) is more pronounced than the long cylinders with $L/d = 2$, 4 (Figs. 3, 11) [28].

For the cylinders with $L/d = 0.5$, although the cross lines could be observed, the cavity phase inversion behavior is not as obvious as the long cylinders. The cavity shrinks and finally contracts into one point in Fig. 13a, b.

As revealed in Fig. 2, for the long cylinder, there is no surface closure, and the splash curtain almost inclines outwards over all the frames. While for the cylinder with $L/d = 2$, the splash curtain has a trend of doming over, which inclines towards inside in Fig. 11a (right view). For the cylinders with $L/d = \{1, 0.5\}$, the splash curtain has almost domed over before the deep closure (Figs. 11b, 13), no more air can flow in the cavity. For the small cylinder with $L/d = 0.5$, the energy transferred to the fluid from the two sides is comparable with that from the two ends, thus the splash curtain formed at the two sides is almost as high as that at the two ends. As air flows into the cavity, the reduced pressure drives the splash to dome over from the four sides.

3.5 The effect of density ratio

For the cylinders with different density, their kinetic energies are different, which will affect the cavity's formation. Similar with the initial horizontal jetting, the value of the density ratio considered here also has little influence on the sprays. We could not observe much difference about the spray between the heavy and the light cylinder (not shown).

Figure 14 shows us the density's effect on the cavity formation and the splash at the time as the cross lines intersect, the velocity of the three cylinders ($L/d = \{4, 2, 1\}$; $D = 0.9$) is $U_0 = 6.22$ m/s. Compared with the case in Fig. 2, several trends can be apparently observed. First, the depth H_{cp} at the cross lines intersection decreases. Second, the depth of the cylinders H as the cross lines intersect decreases. Third, the depth of H_{cp} approaches the depth of the cylinder H as the cross lines intersect. The three trends

Fig. 10 The initial spray jetting formed by the horizontal cylinder with $L/d = 2$ (**a**) and $L/d = 1$ (**b**), both the density ratios are $D = 1.37$ and the initial impact velocities are $U_0 = 6.22$ m/s

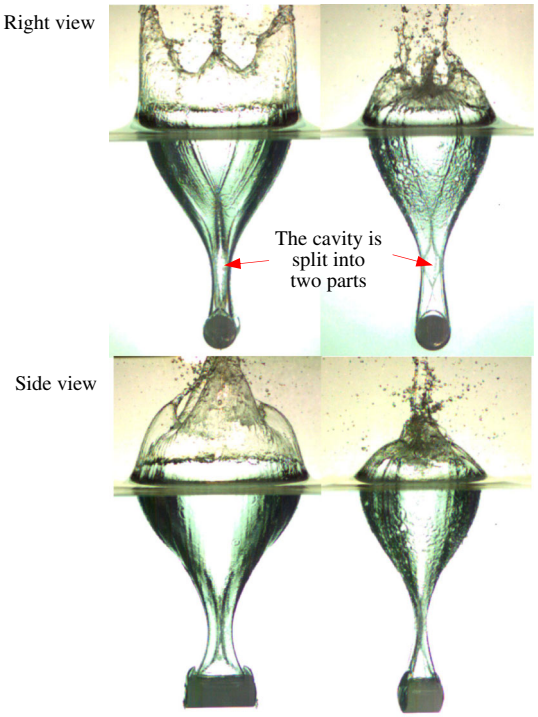

(a) 124ms **(b)** 106ms

Fig. 11 The cavities formed by the cylinder with $L/d = 2$, $D = 1.37$ (**a**) and the cylinder with $L/d = 1$, $D = 1.37$ (**b**), $U_0 = 6.22$ m/s. The *images* in the *two lines* are synchronized in time

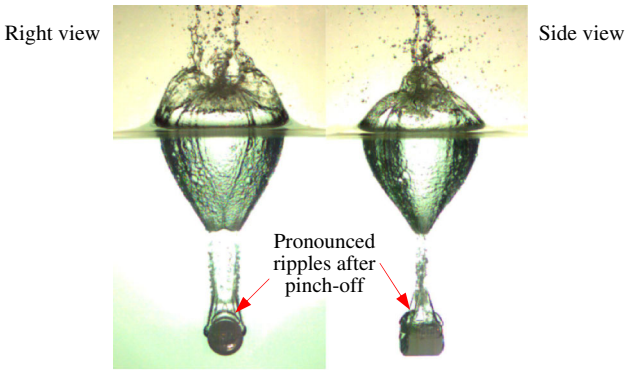

(a) 110ms **(b)** 110ms

Fig. 12 The two snapshots show the same case as that of Fig. 11b, while with 4 ms delay

almost chime with that of low density spheres described by Aristoff et al. [29]. As we pay attention to Fig. 15, we can notice that these cylinders, especially the cylinder with $L/d = 4$, almost could not attract air on the rear surface as the cavity pinches off.

In Fig. 15, the cavity phase inversion behaviors for the light cylinders are almost as evident as the heavy cylinders. The cavities formed by the cylinders with $L/d = \{2, 1\}$ is still cut into two parts (not shown). While if we look at the

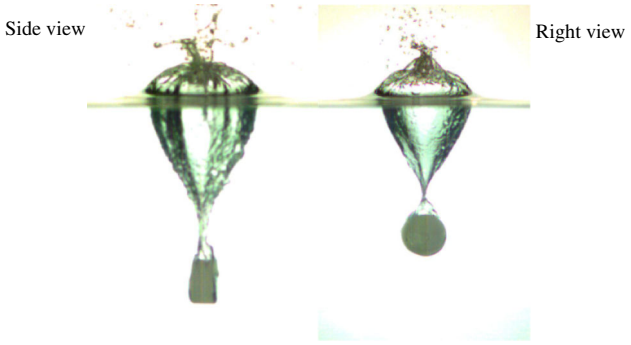

(a) 87ms **(b)** 89ms

Fig. 13 The cavities formed by the cylinder with $L/d = 0.5$, $D = 0.90$ impacting the water surface from a released height of 2.0 m (**a**) and 1.0 m (**b**)

time scale for the motion of the cross lines, some differences could be noticed. For the heavy cylinder with $L/d = 4$, the whole cavity pinches off at 146 ms (Fig. 3j), while it is found a value of 138 ms for the light cylinder (Fig. 15a). For the cylinder with $L/d = 2$, the pinch-off time is 124 ms (Fig. 11a), while it is 120 ms for the light cylinder (Fig. 15b). The pinch-off times for the heavy cylinder and light cylinder with $L/d = 1$ are 106 and 102 ms (Figs. 11b, 15c), respectively. Obviously, the two-dimensional flows at the center disappear earlier for the light cylinders. When the light cylinders pass the water surface, they experience relatively rapid decelerations which could result in an earlier deep closure of the air cavity before it has fully grown.

As to the splash sheath, for the long cylinder with $L/d = 4$, we could not find obvious difference between the heavy cylinder and the light one. The difference occurs for the cylinders with $L/d = \{1, 2\}$. In Fig. 14b, the splash curtain formed by the light cylinder seems to have no trend to close, which inclines outsides. While for the heavy cylinder the splash curtain inclines towards insides in Fig. 11a. For the cylinder with $L/d = 1$, the splash curtain formed by the light cylinder just begins to collapse in Fig. 14c, while for the heavy cylinder, the splash sheath has almost domed over (Fig. 11b). What is more, for both the heavy and light cylinders, it is found that as the parameter of L/d decreases, the height of the splash sheath also decreases.

3.6 The cavity pinch-off

As mentioned in the above sections, one of the most spectacular phenomenon is the evolution of the cross lines. The non-dimensional time and depth at the cross lines intersection is used to reveal the scaling relationship for the cavities.

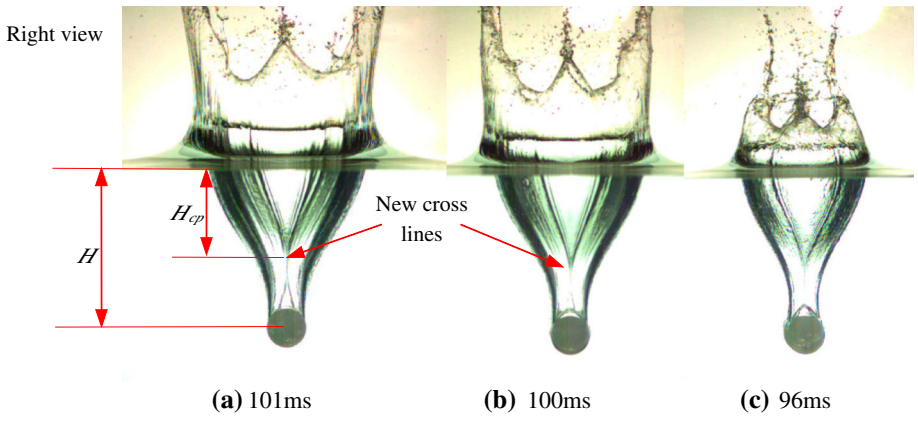

Fig. 14 The snapshots for cavities as the cross lines intersect with each other. They are formed by cylinders with $L/d = 4$ (**a**), $L/d = 2$ (**b**), $L/d = 1$ (**c**), all the initial velocities are $U_0 = 6.22$ m/s, and the density ratio is $D = 0.90$

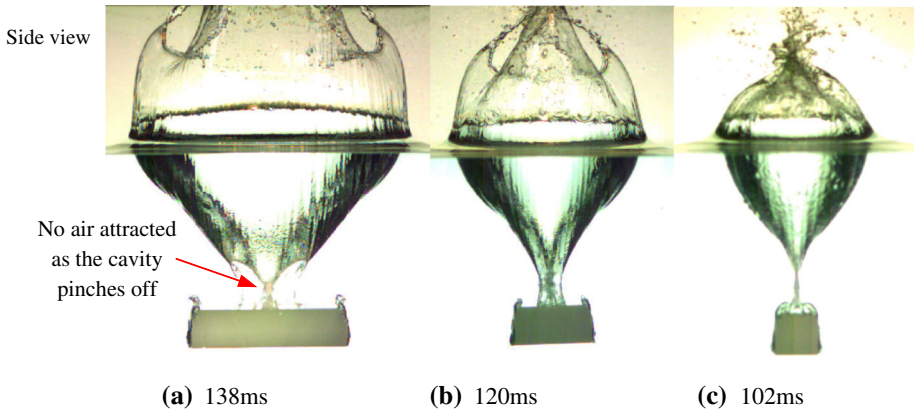

Fig. 15 The images show the side views of the same cases as that in Fig. 14, while with 37 ms (**a**), 20 ms (**b**), and 6 ms (**c**) delay, respectively

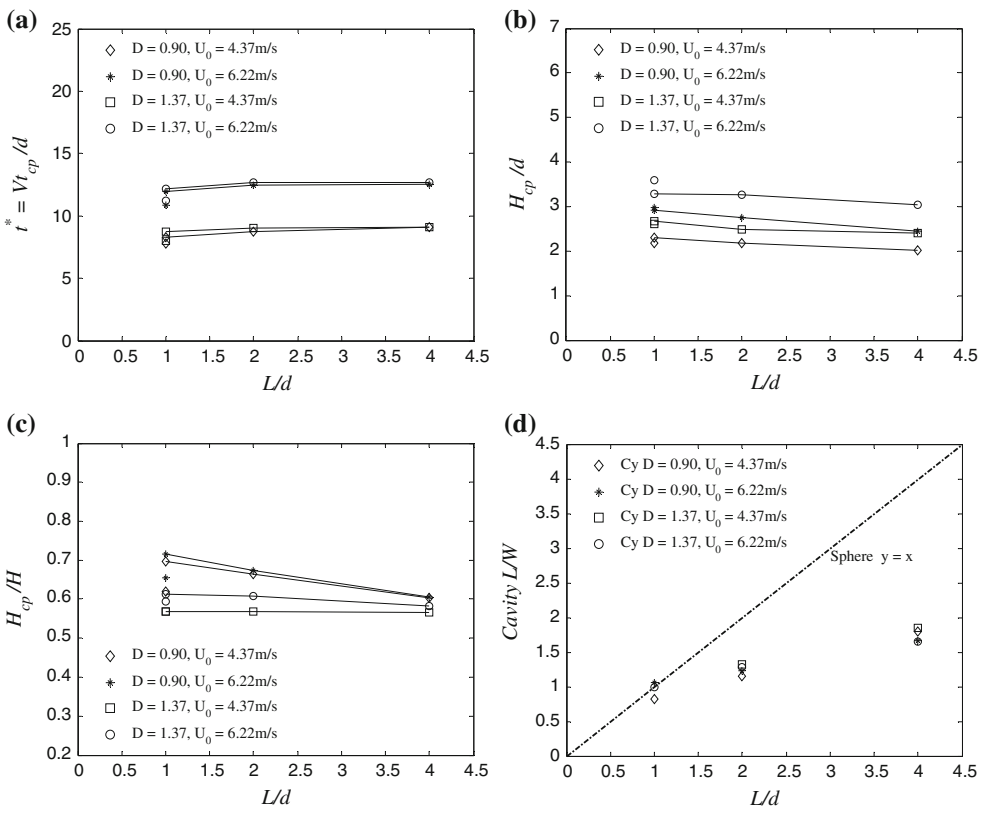

Fig. 16 The characteristics of cavities by the entry of horizontal cylinders. **a** normalized time to the cross lines intersection against the length to diameter ratio of L/d; **b** normalized depth at cross lines intersection as a function of L/d; **c** the ratio of depth at the cross lines intersection to the depth of the object as a function of L/d as the cross lines intersect with each other; **d** the ratio of the cavity's length to width as a function of L/d. Data include all density ratio, L/d and the released height is either 1.0 or 2.0 m. The parameter of L/d for spheres is defined as 1. In **a**, **b**, and **c**, the single data stands for spheres, and the data on the lines stands for these of cylinders

Figure 16a shows the relationship between the non-dimensional time to cross lines intersection, $t^* = Vt_{cp}/d$ versus the L/d. We found as the cylinder's length increases, the non-dimensional time t^* for both the heavy and the light cylinder at the cross lines intersection almost keeps level, with a trend increasing slightly. In addition, the t^* for the spheres is smaller than that for each groups of cylinders with the same density ratio. The non-dimensional time at cross lines intersection has an average value of $\tau = 1.989$, which is intermediate between $\tau = 1.74$ for spheres as reported by Gilbarg and Anderson [22] and $\tau = 2.285 \pm 0.0653$ for disks as reported by Glasheen and McMahon [12].

Figure 16b shows the relationship between non-dimensional depths at the cross lines intersection, H_{cp}/d versus L/d. It is found that as the length of the cylinder increase, the non-dimensional depth at cross lines intersection has a slightly decrease. Figure 16c shows the relationship between the ratios of the depth at the cross lines intersection to the depth of the cylinder as the cross lines intersect with each other, H_{cp}/H versus L/d. We find that the value of H_{cp}/H for heavy cylinders almost level off, while it has a slight decrease for light cylinders. Figure 16d shows the ratio of the cavity's length to its width as the cross lines intersect, L/W versus L/d, that the data for all density ratios, impact velocities almost collapse onto one line. The dashed line in the Fig. 16d is a fitted line of the values L/W for spheres. We could assume that for a cylinder with infinite length, the length of the cavity approximately equals to the length of the cylinder, the width of the cavity is a constant value for given impact velocity, and then the value of L/W just has the linear relationship with the L/d.

3.7 The cylinder trajectory

As the horizontal cylinders enter into water, the end effects will influence the resulting force on them, and thus influence the motion of the cylinders, as well as their trajectories. Both groups of cylinders with $L/d = \{1, 2, 4\}$ and $D = \{0.90, 1.37\}$, are considered. They are released from two heights (1.0 m, 2.0 m) with the center above the water surface, thus the impact velocities are $U_0 = 4.37$ and 6.22 m/s, respectively. The anticipated trend for behaviors of cylinders is that cylinders with different parameters of L/d move with different decelerations as they submerge in water.

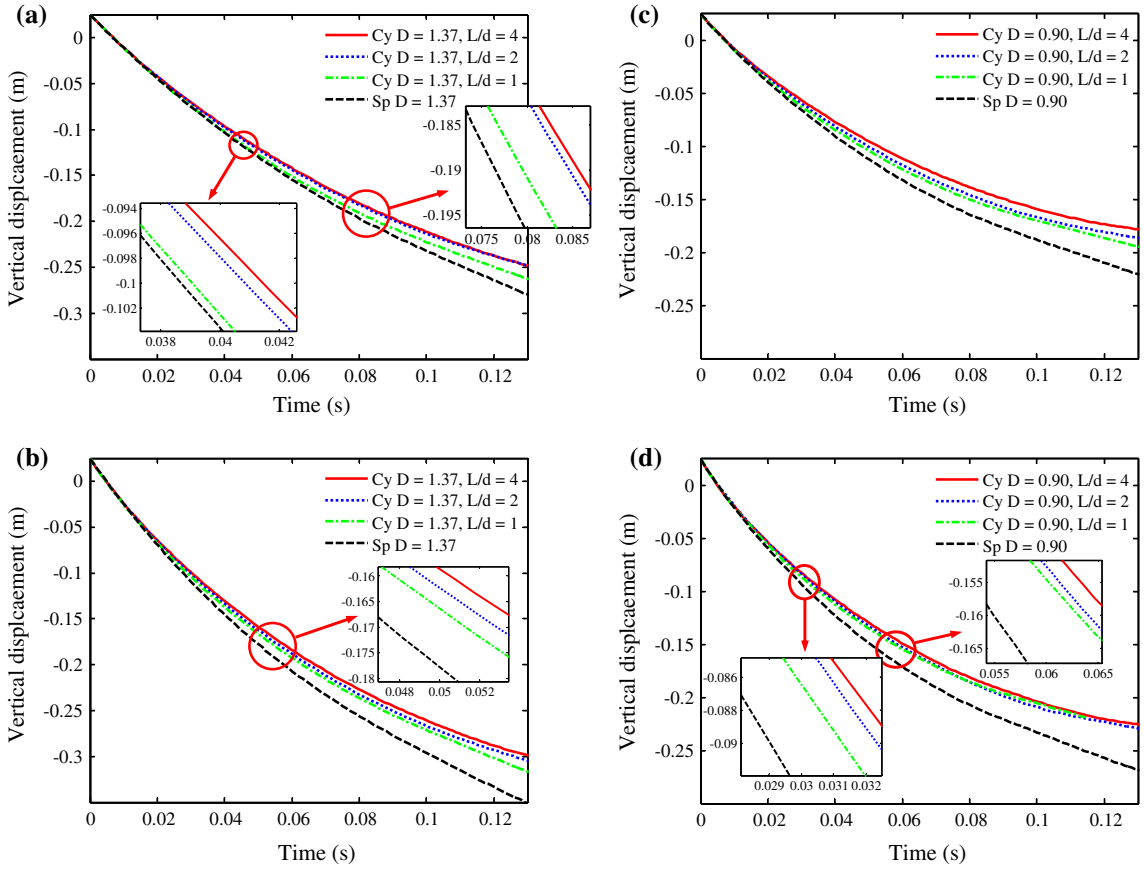

Fig. 17 The trajectory curves of the horizontal cylinders and spheres, **a** the release height is 1.0 m, $D = 1.37$; **b** the release height is 2.0 m, $D = 1.37$; **c** the release height is 1.0 m, $D = 0.9$; **d** the release height is 2.0 m, $D = 0.9$. All density ratios and parameters of L/d are included. *Cy* cylinders, *Sp* sphere

Figure 17 shows the time history for the cylinders and spheres' center as they enters into water, the minus displacement means the position of the center is below the still water surface. In Fig. 17, for each group of cylinders ($L/d = \{1, 2, 4\}$), their trajectory curves show an obvious and similar trends. Cylinders with $L/d = 4$ experience the most rapid deceleration, and the short cylinders with $L/d = 1$ experience the lowest deceleration among them. While for the cylinders with $L/d = 2$, the trajectory curves lie between these of the cylinders with $L/d = \{4, 1\}$.

As regard to the light cylinders, their trajectory curves almost level off (Fig. 17c, d) at the end of the motion. After the light cylinders submerge below the water surface, the buoyant force is positive, they experience relatively rapid deceleration. Their speeds finally drop to zero and then reverse.

In the case of the heavy cylinder, when they are dropped form a height of 1.0 m, the velocity attenuates approximately the same with each other (Fig. 17a); the trend is not as pronounced as other cases.

The trajectory curves of spheres ($d = 50$ mm, $D = \{0.90, 1.37\}$) are also plotted together with each group of cylinders. The spheres are released from the same height (1.0 m, 2.0 m) as the cylinders. We can see from Fig. 17 that when the spheres impact the water surface with the same initial impact velocity as each group of cylinders, they experience much slower deceleration than all the cylinders.

4 Conclusions

Three-dimensional effect on water entry with a horizontal circular cylinder has been studied experimentally. The circular cylinder used in the experiment has the diameter of 50 mm, with the length to diameter ratio varying from 0.5 to 4. A sphere with the diameter of 50 mm is also tested for comparison. Two materials are used for the cylinder resulting in the density ratio of cylinder to water of 1.37 and 0.90. In the experiment a high-speed digital camera system is used. The high quality experimental pictures and the quantitative measurement results on the splashes formed at the initial impact and the cavities formed in the later stage can be used for validation of analytical and numerical methods for three-dimensional water entry. The main findings obtained from this study are summarized as follows.

At the initial stage, the measured jetting speeds for all cylinders are almost the same because the kinetic energy of the flow is focused on the two directions and the flow is nearly two-dimensional. The jetting speed of the horizontal cylinder is about 1.5 times that of the sphere. From the experiment using cylinders with different density ratio it is shown that the cylinder density has small influence on the jetting speed. The initial jetting is relevant to the formation of the cavity behind the cylinders. The critical velocity required to form a complete cavity for a horizontal cylinder is much lower than that for a sphere.

When the cylinder passes through the initial water surface, a cavity is formed and a so-called shape inversion behavior may occur. Different from the case of sphere, the cavity behind a horizontal cylinder is non-axisymmetric, with more complicated behaviors. The shape inversion behavior means that the part of cavity surface at the cross lines is of higher curvature and moves with higher accelerations, finally overtakes the cavity surface with lower curvature. The cavity shape inversion behavior is more obviously seen for the longer cylinders. Other major findings on the effect of L/d are: for the cylinder with $L/d = \{1, 2\}$, the cavity is finally split into two parts as it pinches off; for the cylinders with $L/d = \{4, 2\}$, there is no surface closure; while for cylinder with $L/d = \{1, 0.5\}$, the splash could almost dome over.

Trajectory curves of the cylinders have been obtained from the experimental video record. For same density ratio and initial impact velocity, motion of longer cylinder decelerates more rapidly due to higher drag force by the cavity. The sphere moves at the highest speed. For a horizontal circular cylinder, the three-dimensional effect is important for the trajectory behavior.

Acknowledgments This research was supported by Research Institute for Applied Mechanics, Kyushu University. The authors would like to thank Mr. Makoto Yasunaga, Dr. Sueyoshi Makoto, for their help in designing and installing the experimental setup.

References

1. Worthington AM, Cole RS (1897) Impact with a liquid surface, studied by the aid of instantaneous photography. Philosophical Transactions of the Royal Society A (Containing Papers of a Mathematical or Physical Character) 189:137–1480
2. Watanabe S (1934) Resistance of impact on water surface. Part V-sphere. Scientific Papers of the Institute of Physical and Chemical Research, vol 484, pp 202–208
3. May A, Woodhull JC (1948) Drag coefficients of steel spheres entering water vertically. J Appl Phys 19:1109–1121
4. May A, Woodhull JC (1950) The virtual mass of a sphere entering water vertically. J Appl Phys 21:1285–1289
5. Richardson EG (1948) The impact of a solid on a liquid surface. Proc Phys Soc 4:352–367
6. May A (1951) Effect of surface condition of a sphere on its water-entry cavity. J Appl Phys 22:1219–1222
7. May A (1952) Vertical entry of missiles into water. J Appl Phys 23:1362–1372
8. May A (1975) Water entry and the cavity-running behavior of missiles. Final. Naval Surface Weapons Center White Oak Laboratory, Silver Springs
9. Whalley IA (2002) Project upkeep—a review of the WWII dambuster weapon. In Proceedings of the 38th AIAA/ASME/SAE/ASEE Joint Propulsion Conf. Exhibit. American Institute of Aeronautics and Astronautics Inc., Indianapolis

10. Melosh HJ (1980) Cratering mechanics—observational, experimental, and theoretical. Annu Rev Earth Planet Sci 8:65–93
11. Melosh HJ, Ivanov BA (1999) Impact crater collapse. Annu Rev Earth Planet Sci 27:385–415
12. Glasheen JW, McMahon TA (1996) Vertical water entry of disks at low Froude numbers. Phys Fluids 8:2078–2083
13. Thoroddsen ST, Shen AQ (2001) Granular jets. Phys Fluids 13:4–6
14. Lohse D, Bergmann R, Mikkelsen R, Zeilstra C, van der Meer DM, Versluis M, van der Weele K, van der Hoef M, Kuipers H (2004) Impact on soft sand: void collapse and jet formation. Phys Rev Lett 93(198003):1–4
15. Lohse D, Rauhe R, Bergmann R, van der Meer D (2004) Granular physics: creating a dry variety of quicksand. Nature 432:689–690
16. Rosellini L, Hersen F, Clanet C, Bocquet L (2005) Skipping stones. J Fluid Mech 543:137–146
17. Gekle S, van der Bos A, Bergmann R, van der Meer D, Lohse D (2008) Noncontinuous froude number scaling for the closure depth of a cylindrical cavity. Phys Rev Lett. 100:084502/1–4
18. Bergmann R, van der Meer D, Gekle S, van der Bos A, Lohse D (2009) Controlled impact of a disc on a water surface: cavity dynamics. J Fluid Mech 633:381–409
19. Aristoff JM, Bush JWM (2009) Water entry of small hydrophobic spheres. J Fluid Mech 619:45–78
20. Gekle S, Gordillo JM, van der Meer D, Lohse D (2010) Supersonic air flow due to solid-liquid impact. Phys Rev Lett 104:024501
21. Thoroddsen ST, Etoh TG, Takehara K, Takano Y (2004) Impact jetting by a solid sphere. J Fluid Mech 499:139–148
22. Gilbarg D, Anderson RA (1948) Influence of atmospheric pressure on the phenomena accompanying the entry of spheres into water. J Appl Phys 19:127–139
23. Lee M, Longoria RG, Wilson DE (1997) Cavity dynamics in high-speed water entry. Phys Fluids 9:540
24. Greenhow M, Lin WM (1983) Nonlinear free surface effects: experiment and theory. Rep. 83-19. Department of Ocean Engineering, MIT
25. Truscott TT, Techet AH (2009) Water entry of spinning spheres. J Fluid Mech 625:135–165
26. Enriquez OR, Peters IR, Gekle S, Schmidt LE, van der Meer D, Versluis M, Lohse D (2010) Collapse of nonaxisymmetric cavities. Phys Fluids 22(9):091104
27. Duez C, Ybert C, Clanet C, Bocquet L (2007) Making a splash with water repellency. Nat Phys 3:180–183
28. Grumstrup T, Keller JB, Belmonte A (2007) Cavity ripples observed during the impact of solid objects into liquids. Phys Rev Lett 99:114502
29. Aristoff JM, Truscott TT, Techet AH, Bush JWM (2010) The water entry of decelerating spheres. Phys Fluids 22(3):032102